Electrochimica Acta 98 (2013) 139–145

Contents lists available at SciVerse ScienceDirect

Electrochimica Acta

journal homepage: www.elsevier.com/locate/electacta

N-doped carbon synthesized from N-containing polymers as metal-free catalysts for the oxygen reduction under alkaline conditions

Anqi Zhao[a], Justus Masa[b], Martin Muhler[a], Wolfgang Schuhmann[b], Wei Xia[a,*]

[a] Laboratory of Industrial Chemistry, Ruhr-University Bochum, Germany
[b] Analytische Chemie – Elektroanalytik & Sensorik, Ruhr-University Bochum, Germany

ARTICLE INFO

Article history:
Received 1 September 2012
Received in revised form 4 March 2013
Accepted 9 March 2013
Available online 18 March 2013

Keywords:
Nitrogen-doped carbon
Pyrolysis
Electrocatalysis
Oxygen reduction reaction

ABSTRACT

Nitrogen-doped carbon materials were synthesized and used as metal-free electrocatalysts for the oxygen reduction reaction (ORR) under alkaline conditions. The synthesis was achieved by thermal treatment of nitrogen-containing polymers diluted in different carbon materials. Polypyrrole, polyaniline and polyacrylonitrile were used as N precursors. Carbon black and two types of commercial carbon nanotubes were used as carbon matrices. The obtained N contents were in the range of 1–1.8 wt.%. Different N species including pyridinic, pyrrolic and quaternary N were quantitatively determined by X-ray photoelectron spectroscopy. The ORR activities were evaluated in 0.1 M KOH. Rotating disc electrode studies revealed the presence of multiple active centers in all the samples. The sample obtained using polypyrrole and small diameter nanotubes (ca. 15 nm) had the highest onset potential at −0.07 V vs. Ag/AgCl/3 M KCl, which also showed a significantly higher electrochemical stability than the sample from carbon black and polypyrrole. The ORR activity was not correlated to the total nitrogen amount, but to the amount of pyridinic and quaternary N species. For the onset potential and the $(N_{pyridinic} + N_{quaternary})/N_{total}$ ratio a quasi-linear relation was found, which points to the substantial role of pyridinic- and quaternary-N species in ORR catalysis.

1. Introduction

The oxygen reduction reaction (ORR) under alkaline conditions is an important reaction in alkaline fuel cells [1,2], in metal-air batteries [3] and in chlorine-alkali electrolysis [4]. The development of active, stable and cost-effective ORR electrocatalysts is of vital importance for these processes. Most studies have focused on ORR catalysis in acidic conditions especially in the last ten years [5]. Platinum-based catalysts are among the most widely investigated materials for the ORR under acidic conditions [6,7]. In contrast, silver is known to be a very active and stable catalyst in the ORR under alkaline conditions [8,9]. Bulk silver particles in micrometer dimensions have found applications in the ORR in chlorine-alkali electrolysis [10].

Recently, tremendous efforts have been undertaken to develop cheaper and readily available electrocatalysts for the ORR. Non-noble metal and metal-N_4 catalysts such as transition metal alloys [11] and transition metal N_4-macrocyclic complexes [12,13] have been reported as alternatives to the noble-metal catalysts. Most of these studies are limited to the ORR under acidic conditions. However, N-doped carbon materials as metal-free catalysts are more advantageous in alkaline conditions, where they have demonstrated excellent electrocatalytic activities [14–18]. Gong et al. [19] synthesized vertically aligned N-doped carbon nanotubes (CNTs) with a much higher electrocatalytic activity and long-term stability compared to supported platinum (Pt/C) in alkaline media.

While nitrogen undoubtedly plays an essential role in the activity of the N-doped carbon catalysts, the role of trace metal species has raised considerable debate. The involvement of nitrogen in ORR catalysis dates back to the 1990s, when nitrogen-containing transition metal macrocycles were synthesized using porphyrin complexes and applied in the ORR catalysis under acidic conditions [20,21]. Transition metals are indispensable in this type of ORR catalysts, although they are not necessarily the active centers [22]. There are studies suggesting that the metal species promote the formation of certain nitrogen species, for example, pyridinic groups at edge plane sites, which are the active centers [23–25]. As for nitrogen-doped carbon nanotubes, metal species were not introduced in case of doping by NH_3 treatment [26], or they were washed away before applying as catalysts for the ORR [27]. Hence nitrogen species rather than metal species are often considered as the active centers. However, Atanassov and coworkers [28] believe

* Corresponding author. Fax: +49 234 32 14115.
E-mail address: wei.xia@techem.rub.de (W. Xia).

0013-4686/$ – see front matter © 2013 Elsevier Ltd. All rights reserved.
http://dx.doi.org/10.1016/j.electacta.2013.03.043

that even traces of metallic species could significantly affect the catalytic process. They suggested a two-step process in the ORR catalysis over N-doped carbon materials. Firstly, oxygen is reduced to H_2O_2 by a two electron process catalyzed by nitrogen species. Then, H_2O_2 is transformed to H_2O by disproportionation in a second reaction, which is a heterogeneous catalytic process involving metal species on the surface. Recently, we prepared nitrogen-doped carbon catalysts with exclusive attention on avoiding metal species [29]. The high activity of these catalysts suggested that metal species were not indispensable in ORR catalysis especially under alkaline conditions.

Nitrogen is present on carbon surfaces in different forms, typically pyridinic, pyrrolic, and quaternary or graphite-like nitrogen [30]. The incorporation of nitrogen also leads to the formation of surface defects like edge planes [31,32]. At present, there are still controversies on the role of nitrogen species and surface defects, and the exact nature of active sites of N-doped carbon in the ORR catalysis is still unclear. Earlier studies used to attribute the ORR activity to pyridinic groups at edge plane sites [27,33]. Pyridinic-type nitrogen is believed to be able to promote electron transfer and positively contribute to the ORR catalysis [34]. Several theoretical studies investigated nitrogen atoms at specific sites [35,36], and it was found that not all of the graphite-like N atoms allowed for O_2 adsorption. There are studies suggesting that O_2 is preferentially adsorbed at C sites on zigzag edges adjacent to graphite-like N [35]. Recently, pyrrolic nitrogen was shown to contribute negatively to the activity of nitrogen-doped carbon for the ORR [37,38].

Different methods have been reported for doping carbon materials with nitrogen. N-doped carbon nanotubes can be grown from nitrogen-containing precursors by catalytic chemical vapor deposition [27,39]. Thermal treatment under NH_3 atmosphere is another commonly used method for doping carbon materials with nitrogen [30]. Plasma treatment under nitrogen atmosphere was studied and found to be effective in producing N-doped CNTs [40]. Nitrogen-containing polymers, particularly, polyaniline was coated on CNTs and the obtained composite was thermally treated under an inert atmosphere to get nitrogen-doped CNTs [41].

Here, we report on the synthesis of nitrogen-doped carbon catalysts by thermal treatment of N-containing polymers diluted in different carbon materials. Polypyrrole, polyaniline and polyacrylonitrile were used as nitrogen precursors, and carbon black and different types of CNTs were used as carbon matrices. The obtained N-doped carbon materials were characterized and used as electrocatalysts in the ORR under alkaline conditions.

2. Experimental

2.1. Catalyst synthesis

N-doped carbon catalysts were synthesized by thermal treatment of N-containing polymers diluted in different carbon materials under an inert atmosphere. Polypyrrole (PPy, conductivity 10–40 S/cm), polyaniline (PANI, average $M_w \sim 20{,}000$) and polyacrylonitrile (PAN, average $M_w \sim 150{,}000$) supplied by Aldrich were used as nitrogen precursors. Carbon black (Vulcan XC72, denoted as CB), carbon nanotubes (Applied Sciences Inc. Ohio, USA, denoted as CNTs) and Baytubes C-150P (carbon nanotubes from Bayer MaterialScience AG, Germany, containing traces of Co, Mn, Al, Mg from growth catalyst, denoted as Baytubes) were used as carbon matrices. The CNTs had inner diameters of 20–50 nm, outer diameters of 70–200 nm and a specific surface area of about 30 m^2/g. The Baytubes had inner diameters of 2–6 nm, outer diameters of 13–16 nm and a specific surface area of 280 m^2/g.

As-received CNTs and Baytubes were first washed in 1.5 M HNO_3 under stirring for 72 h at room temperature to remove the residual metal catalysts used in their synthesis. In order to introduce oxygen-containing functional groups, the washed CNTs and Baytubes were functionalized via HNO_3 vapor treatment at 200 °C for 72 h [42]. Different polymers and carbons were mixed by grinding in an agate mortar for 15 min. After testing different polymer to carbon weight ratios, an optimized ratio of 2:5 was used. Thermal treatment was performed by heating the mixtures at 3 K min^{-1} to 800 °C and kept for 180 min under flowing helium. After cooling to room temperature in helium atmosphere, the obtained powders were ground in an agate mortar before further applications. The obtained catalysts with different polymer and carbon combinations were denoted as CB-PPy, CB-PANI, CB-PAN, CNT-PPy and Baytubes-PPy.

2.2. Characterization

Elemental analysis was carried out with a VarioEL analyzer (Elementar Analysensysteme GmbH). X-ray photoelectron spectroscopy (XPS) measurements were carried out in an ultra-high vacuum (UHV) set-up equipped with a monochromatic Al Kα X-ray source (1486.6 eV; anode operating at 14.5 kV and 45 mA) and a high resolution Gammadata-Scienta SES 2002 analyzer. The base pressure in the measurement chamber was maintained at about 7×10^{-10} mbar. The XP spectra were recorded in the fixed transmission mode with a pass energy of 200 eV resulting in an overall energy resolution better than 0.5 eV. Charging effects were compensated by applying a flood gun. The binding energies were calibrated based on the graphite C 1s peak at 284.5 eV. The CASA XPS program with a Gaussian–Lorentzian mix function and Shirley background subtraction was used to analyze the XP spectra quantitatively. The peak positions for all the samples were reproducible using a fixed Gaussian to Lorentz ratio of 70:30 and fixed FWHMs.

2.3. Electrochemical ORR tests

Electrochemical measurements were performed in a conventional three-electrode cell using glassy carbon (⌀ 4 mm; HTW, Germany) modified with N-doped carbon catalyst as the working electrode (WE), Ag/AgCl/3 M KCl as the reference electrode (RE) and Pt foil as the counter electrode (CE). Prior to the experiment, the glassy carbon electrode was polished on polishing cloth using different alumina pastes (3.0, 1.0, 0.3 and 0.05 μm) to obtain a mirror-like surface, followed by ultrasonic cleaning in water. For the preparation of the working electrode, 5.0 mg of the catalyst were dispersed ultrasonically for 30 min in a mixture of water (490 μl), ethanol (490 μl) and Nafion® (5%, 20 μl). 5.3 μl of the resulting catalyst suspension were dropped onto the polished glassy carbon rotating disk electrode and dried in air at room temperature.

Cyclic voltammetry (CV) and rotating disk electrode (RDE) measurements were carried out in argon- and oxygen-saturated 0.1 M KOH solution at room temperature using an Autolab potentiostat/galvanostat (PGSTAT12, Eco Chemie, Utrecht, The Netherlands) in combination with a speed control unit (CTV101) and a rotating disc electrode rotator (EDI101; Radiometer, Villeurbanne, France). All experiments were carried out at room temperature in the potential range of +0.2 to −0.8 V at a scan rate of 5 mV/s after purging with argon or oxygen for 20 min.

3. Results and discussion

3.1. Elemental analysis

Elemental analysis was used to determine the nitrogen content of the obtained nitrogen-doped carbon samples. Among the

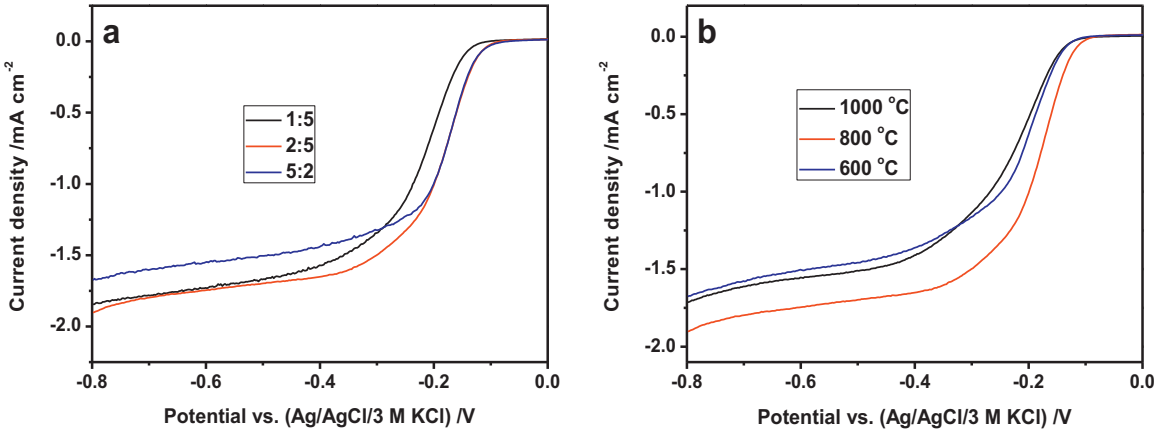

Fig. 1. Linear sweep voltammograms of Baytubes-PPy at a scan rate of 5 mV/s and a rotation rate of 400 rpm. (a) Prepared using different polymer/carbon weight ratios at 800 °C, (b) prepared at different temperatures with constant weight ratio of 2:5.

samples with carbon black as the carbon substrate, CB-PAN exhibited the highest nitrogen loading of 1.81 wt.%, followed by CB-PANI (1.48 wt.%) and CB-PPy (1.02 wt.%) as summarized in Table 1. It can be seen that with the same carbon substrate, the nitrogen loading was related to the molar mass of the initial polymers: a higher polymer molar mass resulted in a higher nitrogen loading after thermal treatment. This correlation suggests that the thermal stability and/or evaporation behavior of polymers play an important role. In addition to chemical nature and crystal structure, molar mass is one of the major factors that affect the thermal stability of polymers, which increases with increase of molar mass. When PPy was used as the N precursor, for the same calculated N content, CNT-PPy showed a higher nitrogen content (1.72 wt.%) than both CB-PPy and Baytubes-PPy, which can be explained by the significantly lower specific surface area of the CNTs used in the CNT-PPy sample. A smaller surface area allowed a more effective coverage of the substrate surface by the polymers due to faster diffusion.

3.2. ORR activity

Nitrogen-doped carbon materials were synthesized by thermal treatment of nitrogen-containing polymers and carbon matrices. To optimize the synthesis conditions, three polymer/carbon weight ratios, namely 1:5, 2:5 and 5:2, and three treatment temperatures, namely, 600, 800 and 1000 °C were tested for polypyrrole and Baytubes. Fig. 1 shows the linear sweep voltammograms measured in O_2-saturated 0.1 M KOH at 5 mV/s and 400 rpm. For the sake of consistency, the onset potential for oxygen reduction was determined when a current density of 0.01 mA cm^{-2} was reached. The sample with a polymer/carbon ratio of 1:5 had the lowest onset potential. For the samples prepared with polymer/carbon ratios of 1:5, 2:5 and 5:2, nitrogen contents were determined to be 0.64 wt.%, 1.25 wt.% and 4.72 wt.%, respectively. However, the onset potential of the sample with a polymer/carbon ratio of 5:2 was found to be similar to that of the sample with a polymer/carbon ratio of 2:5 (Fig. 1a). It can be seen from Fig. 1b that Baytubes-PPy obtained at 800 °C had a higher activity than those at 1000 °C and 600 °C. Hence, all of the samples discussed hereafter were synthesized following the optimized conditions with a polymer/carbon ratio of 2:5 and treatment temperature of 800 °C.

The ORR activity was investigated by cyclic voltammetry in 0.1 M KOH. The measurements were performed in the potential range from 0.2 to −0.8 V at a scan rate of 5 mV/s. All N-doped carbon samples were measured in argon- and oxygen-saturated electrolyte. As a typical example, the first two CV cycles of Baytubes-PPy after preconditioning are shown in Fig. 2. It can be seen that there were no clear redox features in argon-saturated electrolyte. After the electrolyte was saturated with oxygen, a steep increase in the reduction current commencing at about −0.1 V was observed. The CVs of the other four samples, that is, CB-PPy, CB-PANI, CB-PAN and CNT-PPy displayed similar features (not shown).

It can be seen from Fig. 2 that the catalytic current reached a peak maximum at about −0.2 V and decreased as the overpotential was further increased. Additionally, a small kink can be observed on the reduction wave at a potential of about −0.21 V right after the maximum reduction current was reached. This feature was common to all the N-doped carbon catalysts investigated in this study. Taking into account the complexities of surface N species, we attribute this feature to different types of active sites, which are not equally active. Additional active sites can be activated with rising overpotential leading to increasing reduction currents. The relatively

Table 1
Nitrogen contents of N-doped carbon catalysts obtained by elemental analysis. The theoretical nitrogen contents were calculated from the starting mixtures and given for comparison.

Sample	Theoretical nitrogen content (wt.%)	Measured nitrogen content (wt.%)
CB-PPy	6.14	1.02
CB-PANI	4.40	1.48
CB-PAN	7.54	1.81
Baytubes-PPy	6.14	1.25
CNT-PPy	6.14	1.72

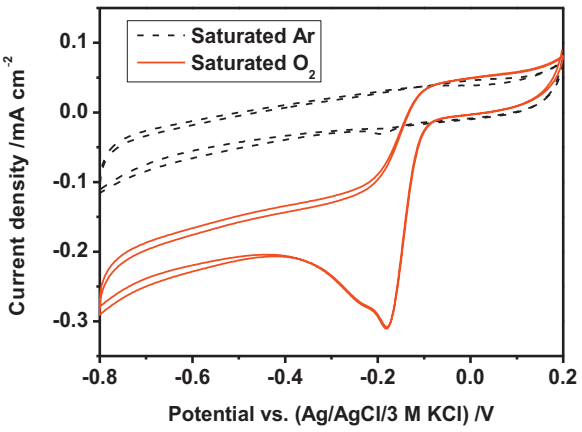

Fig. 2. CVs of Baytubes-PPy recorded at a scan rate of 5 mV/s in argon and oxygen saturated KOH (0.1 M).

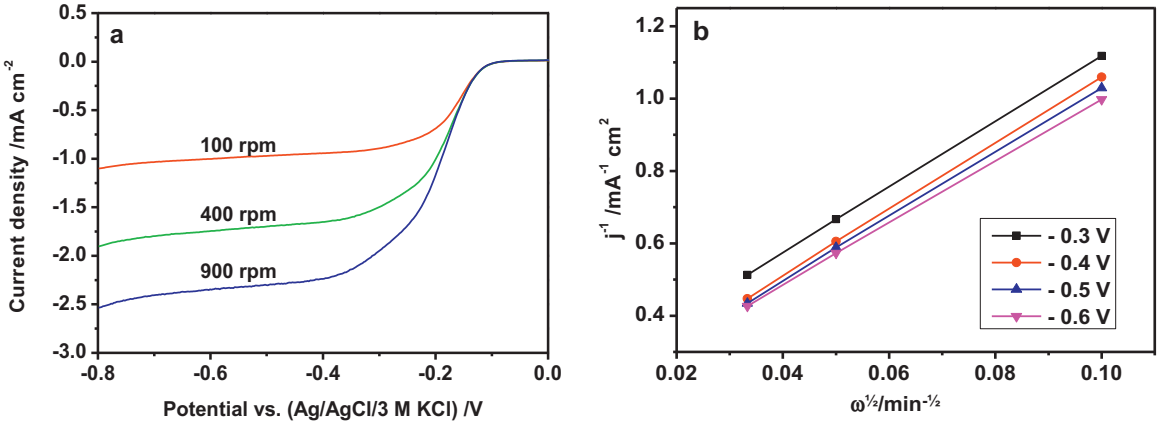

Fig. 3. (a) RDE polarization curves recorded for Baytubes-PPy in O_2-saturated 0.1 M KOH at a scan rate of 5 mV/s and different rotation rates. (b) Koutecky–Levich plot of data extracted from (a).

more active sites which trigger the rapid increase in the reduction current at the onset of the reduction process seem to become less involved at higher overpotentials as the secondary active sites become activated.

The samples were subsequently studied by RDE voltammetry in oxygen-saturated 0.1 M KOH at room temperature. As a typical example, the polarization curves of Baytubes-PPy at different rotation rates are shown in Fig. 3a. It can be seen that the electrocatalytic reduction current density increases with rotation rate from 100 to 900 rpm. The onset potential of the Baytubes-PPy sample was determined to be −0.07 V, which is in good agreement with the value derived from CV measurements. A close inspection of Fig. 3a shows that the reduction curves are characterized by a slight atypical distortion in the mixed kinetic- and diffusion-controlled regions. This distortion should be due to the activation of other active sites of the catalyst as discussed above.

The kinetic parameters were analyzed according to the Koutecky–Levich equation:

$$\frac{1}{J} = \frac{1}{J_k} + \frac{1}{J_l} = \frac{1}{J_k} + \frac{1}{B\sqrt{w}} \quad (1)$$

where J is the measured current density, J_k and J_l are the kinetic- and diffusion-limited current densities, w is the rotation rate (rad s^{-1}) of the electrode. The parameter B is defined as

$$B = 0.62nFC_0 * (D_0)^{2/3} v^{-1/6} \quad (2)$$

where n is the overall number of electrons transferred in oxygen reduction, F is the Faraday constant (F = 96,485 C mol^{-1}), C_0* is the bulk oxygen concentration in the electrolyte, D_0 is the oxygen diffusion coefficient and v is the viscosity of the electrolyte. For an oxygen-saturated 0.1 M KOH solution, $C_0^* = 1.2 \times 10^{-3}$ mol L^{-1}, $D_0 = 1.9 \times 10^{-5}$ cm^2 s^{-1}, and $v = 1.0 \times 10^{-2}$ cm^2 s^{-1} [29].

The corresponding Koutecky–Levich plots for the Baytubes-PPy sample over the potential range from −0.3 V to −0.6 V are shown in Fig. 3b. The electron transfer number (n) for the different catalysts was calculated from the slope of the Koutecky–Levich plots, in accordance with Eqs. (1) and (2).

For the Baytubes-PPy sample, the value of n was derived to be 3.25 at −0.5 V, suggesting a higher selectivity for four-electron transfer in the ORR. The Koutecky–Levich plots at different potentials in Fig. 3b are not necessarily parallel. Linearity and parallelism of Koutecky–Levich plots at different potentials indicate that the mechanism of the ORR, specifically, the number of electrons exchanged does not change in the given potential range and the reaction is of first order with respect to the oxygen concentration. The evident change, albeit small, in the slope of the curves in Fig. 3b shows that there is a slight change in the number of electrons transferred as the potential is changed. This is to be expected given the fact that the catalyst surface has various active sites with different activities.

As mentioned in Section 2, the Baytubes were thoroughly washed with diluted HNO_3 to leach out the residual metal species used in their synthesis. For comparison, a Baytubes-PPy sample without washing was also synthesized following the same procedure. The nitrogen content was determined to be 1.17 wt.% by elemental analysis. However, this sample appeared to be slightly less active than the washed sample. Hence, we have no evidence that the residual metal enhanced the ORR activity under applied conditions, and the role of metal species will not be considered in the following discussion. It is worth to note that the CNTs and Baytubes were washed in dilute HNO_3 for the synthesis of all the samples discussed hereafter. However, we cannot fully exclude the presence of metal species and their possible contribution to ORR catalysis.

Linear sweep voltammograms of all the five samples obtained at a rotation rate of 100 rpm are shown in Fig. 4. Pure carbon black and two types of carbon nanotubes without nitrogen were included for comparison. The reasons why the diffusion-limited currents are not well defined have been explained in the preceding sections. The reduction of oxygen at all the samples occurred under mixed kinetic/diffusion control in the potential region between 0.0 and −0.3 V, but was mostly under diffusion control for potentials below −0.3 V. It can be seen that pure CB is less active than the N-doped samples as indicated by a lower onset potential and lower current densities. Obviously, the incorporation of nitrogen is essential for the ORR activity of the carbon materials. Among the N-doped carbon black samples, the CB-PPy sample, which also had the lowest nitrogen content (1.02 wt.%), showed a higher ORR activity than CB-PAN (1.81 wt.%) and CB-PANI (1.48 wt.%) on the basis of their onset potentials. The onset potentials of all the samples followed the order CB-PPy > CB-PAN > CB-PANI > CB (Fig. 4a). Therefore, the ORR activity cannot be directly correlated to the measured nitrogen content (Table 1).

The ORR activities of samples obtained with PPy as the N-containing precursor and corresponding carbon materials are shown in Fig. 4b. It can be found that the activities of all the carbon materials increased after incorporation of nitrogen, and the Baytubes exhibited a higher onset potential than carbon black and CNT. As compared to CB-PPy, for the different carbon sources, CNT-PPy showed an inferior performance with a lower onset potential and

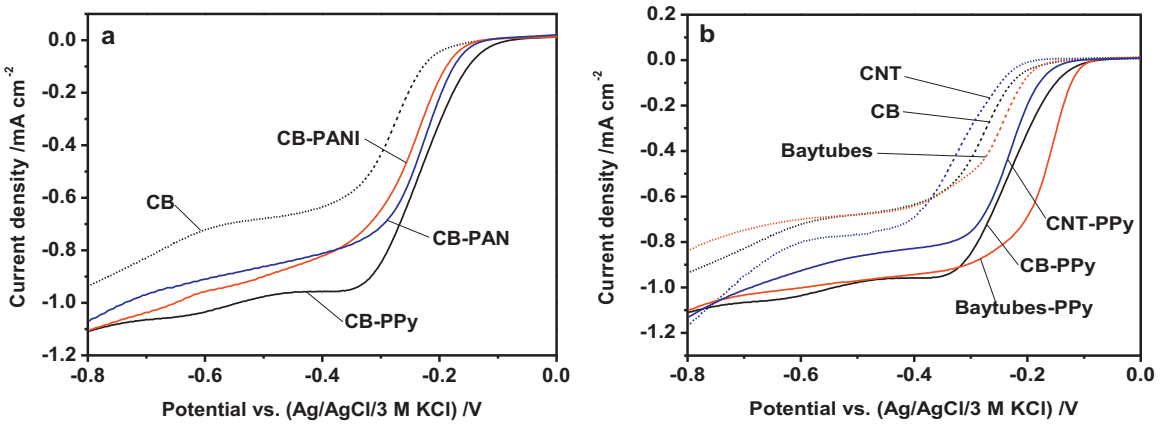

Fig. 4. Linear sweep voltammograms of N-doped carbon black using different N precursors (a) and N-doped carbon using PPy as precursor (b) at a scan rate of 5 mV/s and a rotation rate of 100 rpm.

lower current densities at $E > -0.3$ V. In contrast, the Baytubes-PPy sample exhibited higher onset potential and clearly higher current densities.

Overall, the ORR activities increase in the order CB-PANI < CNT-PPy < CB-PAN < CB-PPy < Baytubes-PPy as determined by onset potential. Despite the superior performance of Baytubes-PPy, it is important to note that the N content was lower in Baytubes-PPy than in all the other samples except for CB-PPy. Obviously, the total nitrogen content is not directly correlated to the catalytic activity of N-doped carbon catalysts. Hence, the influence of the type of N-containing groups on ORR activities was analyzed by XPS.

3.3. XPS studies

High-resolution XPS measurements were performed using the nitrogen-doped carbon samples. In the survey spectra only C, O and N were detected, and metallic species were absent. Taking into account the washing procedure applied before the sample synthesis, the presence of metallic species on the surface of the samples can be excluded. The region spectra were normalized to the intensity of the C 1s peak of graphitic carbon at 284.5 eV. The XP O 1s spectra of all the samples were measured. However, we did not observe significant differences that can be correlated to their catalytic performance. It is not clear at this stage how the oxygen groups influence the ORR catalysis. Fig. 5 shows the deconvoluted XP N 1s spectra of the nitrogen-doped carbon samples. The N 1s spectra of CB-PPy and Baytubes-PPy appear to be very weak. All the samples show two main contributions in the N 1s region, which were decomposed into three peaks at binding energies of 398.3 eV (N1), 400.5 eV (N2), and 401.5 eV (N3), assigned to pyridinic-, pyrrolic-, and quaternary-type nitrogen groups, respectively [43,44]. Only traces of nitrogen were detected in the CB-PPy sample as indicated by the weak N 1s peaks. The Baytubes-PPy sample also showed relatively low N 1s peak intensities (Fig. 5b), indicating a low surface atomic concentration of N.

The surface atomic compositions were derived from the XPS region scans. As compared to the weight loading determined by elemental analysis (Table 1), the nitrogen content determined by XPS studies reflects the atomic concentration on the surface. It can be seen from the N/C ratios listed in Table 2 that the XPS studies showed a similar trend as the elemental analysis. Among all the five samples, the lowest N/C ratio of 0.20×10^{-2} was derived for the CB-PPy sample, with the Baytubes-PPy sample showing a higher N/C ratio of 0.63×10^{-2}. In contrast, the other three samples showed considerably higher nitrogen contents on the surface.

Further quantitative analysis of the N 1s spectra was carried out to determine the content of the different nitrogen-containing groups in the nitrogen-doped carbon materials. The calculated relative concentrations of pyridinic-, pyrrolic-, and quaternary-type nitrogen are summarized in Table 2. It can be seen that the Baytubes-PPy sample had the highest concentration (50%) of

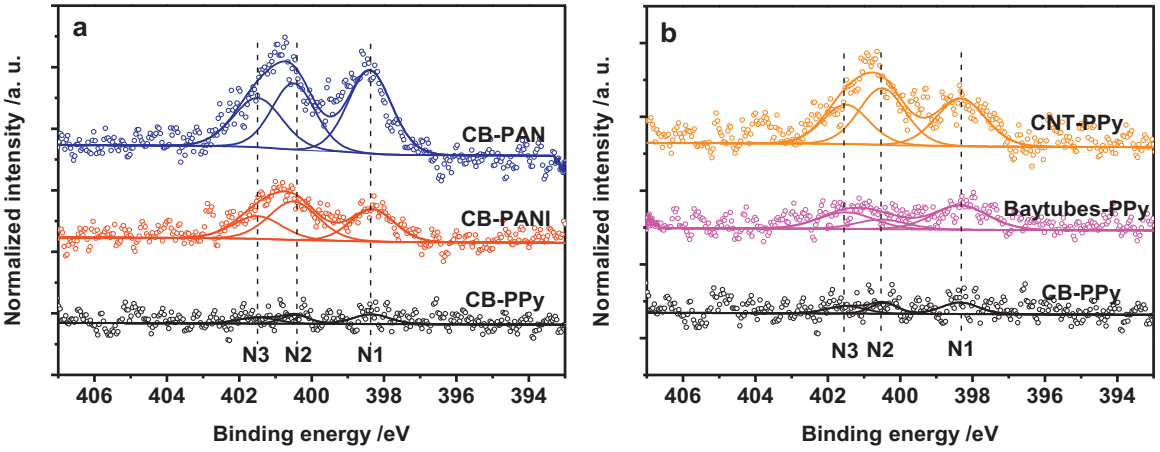

Fig. 5. XP N 1s spectra of N-doped carbon black using different N precursors (a) and N-doped carbon using PPy as N precursor (b). The sample CB-PPy is shown in both (a) and (b) for comparison.

Table 2
N/C ratios and relative concentrations of different nitrogen groups obtained by deconvolution of the XP N 1s spectra and oxygen reduction onset potential of nitrogen-doped carbon. N1: pyridinic-N; N2: pyrrolic-N; N3: quaternary-N.

Sample	N/C (10^{-2})	N1 (%)	N2 (%)	N3 (%)	$(N1+N3)/N_{total}$	Onset potential (V)
CB-PPy	0.20	43	29	28	0.71	−0.08
CB-PANI	1.02	32	43	25	0.57	−0.14
CB-PAN	1.95	41	32	27	0.68	−0.11
Baytubes-PPy	0.63	50	17	33	0.83	−0.07
CNT-PPy	1.30	35	39	26	0.61	−0.12

pyridinic-N groups (N1), followed by CB-PPy with 43%. In contrast, the CB-PANI sample had the highest amount (43%) of pyrrolic-N groups (N2). Moreover, the Baytubes-PPy also displayed the highest amount of quaternary-N groups (N3) of 33%.

Previous studies suggested that pyridinic-type nitrogen could improve the ORR activity due to the conjugation effect of the nitrogen lone pair electrons and the graphene π system [34,36]. Computer simulations support this hypothesis, and also show that the existence of graphite-type nitrogen enhances O_2 adsorption at C sites on the edges located nearby graphite-type nitrogen [35]. Hence, the pyridinic-N and quaternary-N were considered in tandem, and the ratios of $(N1+N3)/N_{total}$ of the different samples are listed in Table 2 together with their onset potentials in the ORR. Surprisingly, the ratio correlates well with ORR activities. A higher $(N1+N3)/N_{total}$ ratio led to a higher onset potential and vice versa with a quasi-linear relation (Fig. 6). This linear relation cannot be considered as conclusive quantitative judgment due to the complexity of ORR catalysis. However, it does point to the substantial contributions of pyridinic- and quaternary-N species, presumably by promoting electron transfer and O_2 adsorption in ORR catalysis. When H_2SO_4 is used as electrolyte, although the existence of quaternary-N species can increase O_2 adsorption, adsorption of SO_4^{2-} anions on the surface of the electrode reduces the available adsorption sites for oxygen [45]. Pyridinic-N species may therefore be considered to be primarily responsible for enhanced ORR activity. In alkaline electrolytes, quaternary-N species have been established to play a superior role compared to pyridinic-N in promoting ORR, which has led many researchers to overlook the role of pyridinic-N. In fact, both pyridinic- and quaternary-N species improve the catalytic activity of oxygen reduction. On the contrary, pyrrolic nitrogen did not contribute to the electrocatalytic activity, which is in good agreement with reported results [37,38].

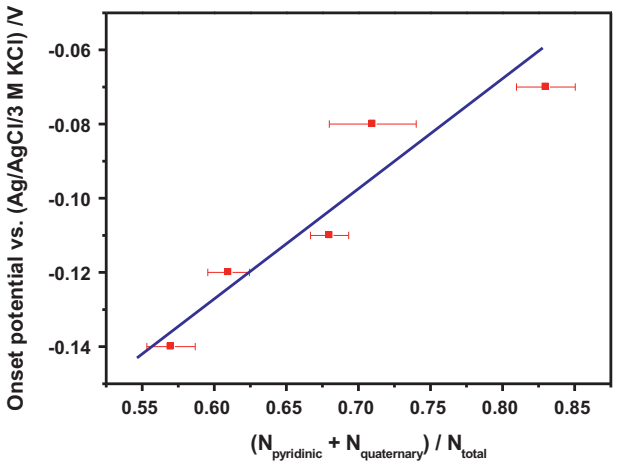

Fig. 6. $(N1+N3)/N_{total}$ ratio of nitrogen-containing groups in nitrogen-doped carbon catalysts versus ORR onset potential in 0.1 M KOH.

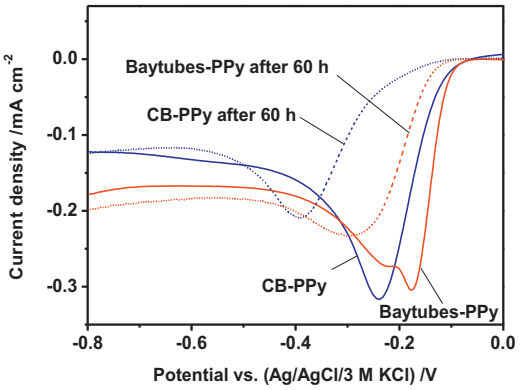

Fig. 7. Linear sweep voltammograms of Baytubes-PPy and CB-PPy before and after stability tests measured in O_2-saturated 0.1 M KOH at a scan rate of 5 mV/s.

3.4. Stability test

Two samples with the best ORR activities, i.e., Baytubes-PPy and CB-PPy, were selected for electrochemical stability studies. Fig. 7 shows the linear sweep voltammograms of Baytubes-PPy and CB-PPy before and after 60 h in O_2-saturated 0.1 M KOH solution. There were clear changes in the onset potential and current density for both samples after the stability tests. However, CB-PPy showed more pronounced degradation of catalytic performance as indicated by a larger shift of the onset potential and decrease of current density. The difference can be undoubtedly assigned to the structural difference of the carbon matrices used in the synthesis. Baytubes with ordered graphitic structure are more stable than the amorphous carbon black, which is in good agreement with our earlier studies [46]. The high stability of the Baytubes-PPy proves its high potential in ORR catalysis under alkaline conditions.

4. Conclusions

N-doped carbon electrocatalysts were synthesized by thermal treatment of nitrogen-containing polymers and carbon mixtures. The N contents were obtained in the range of 1 to 1.8 wt.%. The N/C atomic ratios in the near-surface region were found to be in the range of 0.2 to 2% as derived from XPS measurements. RDE studies revealed the presence of multiple active centers in all the samples. Comparative studies indicate that residual metal species did not have positive effects on the ORR under the applied conditions. The sample obtained using polypyrrole and CNTs (Baytubes) showed the highest onset potential at −0.07 V vs Ag/AgCl/3 M KCl, which also showed a significantly higher electrochemical stability than the sample from carbon black and polypyrrole. The onset potential and the $(N_{pyridinic}+N_{quaternary})/N_{total}$ ratio showed a quasi-linear behavior, suggesting that the ORR activity was not correlated to the total nitrogen amount, but to the concentration of pyridinic and quaternary N species, which points to the substantial role of pyridinic- and quaternary-N species in ORR catalysis.

Acknowledgements

A. Zhao thanks the China Scholarship Council for a research grant. Justus Masa is grateful to the German Academic Exchange Service (DAAD) for a PhD scholarship.

References

[1] J.S. Spendelowa, A. Wieckowski, Electrocatalysis of oxygen reduction and small alcohol oxidation in alkaline media, Physical Chemistry Chemical Physics 9 (2007) 2654.
[2] J. Guo, A. Hsu, D. Chu, R. Chen, Improving oxygen reduction reaction activities on carbon-supported Ag nanoparticles in alkaline solutions, Journal of Physical Chemistry C 114 (2010) 4324.
[3] J.-S. Lee, S.T. Kim, R. Cao, N.-S. Choi, M. Liu, K.T. Lee, J. Cho, Metal-air batteries with high energy density: Li-air versus Zn-air, Advanced Energy Materials 1 (2011) 34.
[4] L. Lipp, S. Gottesfeld, J. Chlistunoff, Peroxide formation in a zero-gap chlor-alkali cell with an oxygen-depolarized cathode, Journal of Applied Electrochemistry 35 (2005) 1015.
[5] M. Winter, R.J. Brodd, What are batteries, fuel cells, and supercapacitors? Chemical Reviews 104 (2004) 4245.
[6] X. Yu, S. Ye, Recent advances in activity and durability enhancement of Pt/C catalytic cathode in PEMFC: part II: degradation mechanism and durability enhancement of carbon supported platinum catalyst, Journal of Power Sources 172 (2007) 145.
[7] Z. Chen, M. Waje, W. Li, Y. Yan, Supportless Pt and PtPd nanotubes as electrocatalysts for oxygen-reduction reactions, Angewandte Chemie 119 (2007) 4138.
[8] Y. Lu, W. Chen, Size effect of silver nanoclusters on their catalytic activity for oxygen electro-reduction, Journal of Power Sources 197 (2012) 107.
[9] G.K.H. Wiberg, K.J.J. Mayrhofer, M. Arenz, Investigation of the oxygen reduction activity on silver – a rotating disc electrode study, Fuel Cells 10 (2010) 575.
[10] M. Sudoh, K. Arai, Y. Izawa, T. Suzuki, M. Uno, M. Tanaka, K. Hirao, Y. Nishiki, Evaluation of Ag-based gas-diffusion electrode for two-compartment cell used in novel chlor-alkali membrane process, Electrochimica Acta 56 (2011) 10575.
[11] B. Wang, Recent development of non-platinum catalysts for oxygen reduction reaction, Journal of Power Sources 152 (2005) 1.
[12] R. Bashyam, P. Zelenay, A class of non-precious metal composite catalysts for fuel cells, Nature 443 (2006) 63.
[13] M. Lefèvre, E. Proietti, F. Jaouen, J.-P. Dodelet, Iron-based catalysts with improved oxygen reduction activity in polymer electrolyte fuel cells, Science 324 (2009) 71.
[14] Y. Tang, B.L. Allen, D.R. Kauffman, A. Star, Electrocatalytic activity of nitrogen-doped carbon nanotube cups, Journal of the American Chemical Society 131 (2009) 13200.
[15] C.V. Rao, Y. Ishikawa, Activity, selectivity, and anion-exchange membrane fuel cell performance of virtually metal-free nitrogen-doped carbon nanotube electrodes for oxygen reduction reaction, Journal of Physical Chemistry C 116 (2012) 4340.
[16] D. Higgins, Z. Chen, Z. Chen, Nitrogen doped carbon nanotubes synthesized from aliphatic diamines for oxygen reduction reaction, Electrochimica Acta 56 (2011) 1570.
[17] Z. Wang, R. Jia, J. Zheng, J. Zhao, L. Li, J. Song, Z. Zhu, Nitrogen-promoted self-assembly of N-doped carbon nanotubes and their intrinsic catalysis for oxygen reduction in fuel cells, ACS Nano 5 (2011) 1677.
[18] Y. Ma, L. Sun, W. Huang, L. Zhang, J. Zhao, Q. Fan, W. Huang, Three-dimensional nitrogen-doped carbon nanotubes/graphene structure used as a metal-free electrocatalyst for the oxygen reduction reaction, Journal of Physical Chemistry C 115 (2011) 24592.
[19] K. Gong, F. Du, Z. Xia, M. Durstock, L. Dai, Nitrogen-doped carbon nanotube arrays with high electrocatalytic activity for oxygen reduction, Science 323 (2009) 760.
[20] M. Bron, J. Radnik, M. Fieber-Erdmann, P. Bogdanoff, S. Fiechter, EXAFS, XPS and electrochemical studies on oxygen reduction catalysts obtained by heat treatment of iron phenanthroline complexes supported on high surface area carbon black, Journal of Electroanalytical Chemistry 535 (2002) 113.
[21] G. Lalande, R. Cote, D. Guay, J.P. Dodelet, L.T. Weng, P. Bertrand, Is nitrogen important in the formulation of Fe-based catalysts for oxygen reduction in solid polymer fuel cells? Electrochimica Acta 42 (1997) 1379.
[22] J. Masa, T. Schilling, M. Bron, W. Schuhmann, Electrochemical synthesis of metal-polypyrrole composites and their activation for electrocatalytic reduction of oxygen by thermal treatment, Electrochimica Acta 60 (2012) 410.
[23] R. Liu, C.V. Malotki, L. Arnold, N. Koshino, H. Higashimura, M. Baumgarten, K. Mullen, Triangular trinuclear metal-N4 complexes with high electrocatalytic activity for oxygen reduction, Journal of the American Chemical Society 133 (2011) 10372.
[24] K. Wiesener, N4-chelates as electrocatalyst for cathodic oxygen reduction, Electrochimica Acta 31 (1986) 1073.
[25] J. Yang, D.-J. Liu, N.N. Kariuki, L.X. Chen, Aligned carbon nanotubes with built-in FeN4 active sites for electrocatalytic reduction of oxygen, Chemical Communications (2008) 329.
[26] T.C. Nagaiah, S. Kundu, M. Bron, M. Muhler, W. Schuhmann, Nitrogen-doped carbon nanotubes as a cathode catalyst for the oxygen reduction reaction in alkaline medium, Electrochemistry Communications 12 (2010) 338.
[27] S. Kundu, T.C. Nagaiah, W. Xia, Y. Wang, S.V. Dommele, J.H. Bitter, M. Santa, G. Grundmeier, M. Bron, W. Schuhmann, M. Muhler, Electrocatalytic activity and stability of nitrogen-containing carbon nanotubes in the oxygen reduction reaction, Journal of Physical Chemistry C 113 (2009) 14302.
[28] T.S. Olson, S. Pylypenko, J.E. Fulghum, P. Atanassov, Bifunctional oxygen reduction reaction mechanism on non-platinum catalysts derived from pyrolyzed porphyrins, Journal of the Electrochemical Society 157 (2010) B54.
[29] W. Xia, J. Masa, M. Bron, W. Schuhmann, M. Muhler, Highly active metal-free nitrogen-containing carbon catalysts for oxygen reduction synthesized by thermal treatment of polypyridine-carbon black mixtures, Electrochemistry Communications 13 (2011) 593.
[30] S. Kundu, W. Xia, W. Busser, M. Becker, D.A. Schmidt, M. Havenith, M. Muhler, The formation of nitrogen-containing functional groups on carbon nanotube surfaces: a quantitative XPS and TPD study, Physical Chemistry Chemical Physics 12 (2010) 4351.
[31] S. Maldonado, S. Morin, K.J. Stevenson, Structure, composition, and chemical reactivity of carbon nanotubes by selective nitrogen doping, Carbon 44 (2006) 1429.
[32] J.D. Wiggins-Camacho, K.J. Stevenson, Effect of nitrogen concentration on capacitance, density of states, electronic conductivity, and morphology of N-doped carbon nanotube electrodes, Journal of Physical Chemistry C 113 (2009) 19082.
[33] C.V. Rao, C.R. Cabrera, Y. Ishikawa, In search of the active site in nitrogen-doped carbon nanotube electrodes for the oxygen reduction reaction, Journal of Physical Chemistry Letters 1 (2010) 2622.
[34] R.A. Sidik, A.B. Anderson, N.P. Subramanian, S.P. Kumaraguru, B.N. Popov, O_2 reduction on graphite and nitrogen-doped graphite: experiment and theory, Journal of Physical Chemistry B 110 (2006) 1787.
[35] T. Ikeda, M. Boero, S.-F. Huang, K. Terakura, M. Oshima, J.-i. Ozaki, Carbon alloy catalysts: active sites for oxygen reduction reaction, Journal of Physical Chemistry C 112 (2008) 14706.
[36] K.A. Kurak, A.B. Anderson, Nitrogen-treated graphite and oxygen electroreduction on pyridinic edge sites, Journal of Physical Chemistry C 113 (2009) 6730.
[37] K. Artyushkova, S. Pylypenko, T.S. Olson, J.E. Fulghum, P. Atanassov, Predictive modeling of electrocatalyst structure based on structure-to-property correlations of X-ray photoelectron spectroscopic and electrochemical measurements, Langmuir 24 (2008) 9082.
[38] J.D. Wiggins-Camacho, K.J. Stevenson, Mechanistic discussion of the oxygen reduction reaction at nitrogen-doped carbon nanotubes, Journal of Physical Chemistry C 115 (2011) 20002.
[39] S.V. Dommele, A. Romero-Izquirdo, R. Brydson, K.P.D. Jong, J.H. Bitter, Tuning nitrogen functionalities in catalytically grown nitrogen-containing carbon nanotubes, Carbon 46 (2008) 138.
[40] R. Chetty, S. Kundu, W. Xia, M. Bron, W. Schuhmann, V. Chirila, W. Brandl, T. Reinecke, M. Muhler, PtRu nanoparticles supported on nitrogen-doped multiwalled carbon nanotubes as catalyst for methanol electrooxidation, Electrochimica Acta 54 (2009) 4208.
[41] C. Jin, T.C. Nagaiah, W. Xia, B. Spliethoff, S. Wang, M. Bron, W. Schuhmann, M. Muhler, Metal-free electrocatalytically active nitrogen-doped carbon nanotubes synthesized by coating with polyaniline, Nanoscale 2 (2010) 981.
[42] W. Xia, C. Jin, S. Kundu, M. Muhler, A highly efficient gas-phase route for the oxygen functionalization of carbon nanotubes based on nitric acid vapor, Carbon 47 (2009) 919.
[43] J. Casanovas, J.M. Ricart, J. Rubio, F. Illas, J.M. Jime'nez-Mateos, Origin of the large N 1s binding energy in X-ray photoelectron spectra of calcined carbonaceous materials, Journal of the American Chemical Society 118 (1996) 8071.
[44] Z. Yang, Y. Xia, R. Mokaya, Aligned N-doped carbon nanotube bundles prepared via CVD using zeolite substrates, Chemistry of Materials 17 (2005) 4502.
[45] J.X. Wang, N.M. Markovic, R.R. Adzic, Kinetic analysis of oxygen reduction on Pt(1 1 1) in acid solutions: intrinsic kinetic parameters and anion adsorption effects, Journal of Physical Chemistry B 108 (2004) 4127.
[46] J. Masa, A. Bordoloi, M. Muhler, W. Schuhmann, W. Xia, Enhanced electrocatalytic stability of platinum nanoparticles supported on a nitrogen-doped composite of carbon nanotubes and mesoporous titania under oxygen reduction conditions, ChemSusChem 5 (2012) 523.